

Unravel the Active Site in Nitrogen-Doped Double-Walled Carbon Nanotubes for Nitrogen Dioxide Gas Sensor

Worawut Muangrat, Winadda Wongwiriyan, Visittapong Yordsri, Thanattha Chobsilp, Saowaluk Inpaeng, Chaisak Issro, Oleg Domanov, Paola Ayala, Thomas Pichler, and Lei Shi*

In this paper, a nitrogen dioxide (NO₂) gas sensor using nitrogen-doped double-walled carbon nanotubes (N-DWCNTs) with different types of nitrogen is demonstrated, and the sensor performance to the pyridinic nitrogen is related. The ratio of nitrogen is controlled by the temperature applied for the synthesis. It is found that the fabricated sensor from N-DWCNTs enable an approximately threefold improvement in NO₂ detection compared to the sensor from DWCNTs. Also, the improvement of sensor response of N-DWCNTs more depends on the pyridinic site than the other types of nitrogen, because it can strongly interact with the NO₂ molecule. The sensing mechanism is attributed to the charge transfer between the NO₂ molecule and the sensing materials (especially with pyridinic site), which shifts the Fermi level, resulting in a decrease of the electrical resistance. Furthermore, the relation between the sensor response and the concentration of NO₂ is derived based on Langmuir adsorption isotherm, and the calculated detection limit can be down to 0.14 ppm, which suggests that the N-DWCNTs-based sensor is a promising approach for low concentration NO₂ detection at room temperature.

1. Introduction

Carbon nanotubes (CNTs) is an allotrope of carbon with a cylindrical nanostructure.^[1,2] The excellent structural, mechanical, thermal, and electrical properties of CNTs make them a promising candidate for the potential applications.^[3] For example, CNTs have been shown outstanding potential for gas sensing application because of their large specific area^[4] and high electrical conductivity.^[5,6] Single-wall CNTs (SWCNTs) and multi-walled CNTs (MWCNTs)-based sensor have demonstrated a high response to oxidizing gas down to parts per million (ppm) level under room-temperature operation,^[6–10] especially to the nitrogen dioxide (NO₂). NO₂ is a toxic gas that can cause nausea, irritation to the eyes, nose, and throat, as well as damage the lungs and may lead to chronic bronchitis. Therefore, detection of the NO₂ below the risk range is absolutely crucial. Most studies on the enhanced NO₂


gas-sensing performance have focused on the combining polymer functionalization or metal nanoparticle decoration with CNTs.^[11–15] The CNTs functionalized polymer and decorated metal nanoparticle show high sensitivity to NO₂. Recently, another approach for improvement of the sensitivity is doping the CNTs with heteroatoms. Doping CNTs with boron or nitrogen into CNT structure can enhance the performance toward various gases.^[16–18] Also, N-CNTs could be more efficient for detection of toxic species compared to undoped CNTs.^[16] In addition, N-MWCNTs have shown slightly better carbon monoxide sensitivity than the B-MWCNTs.^[17] However, since many types of nitrogen usually exist in the N-CNTs, the roles of these nitrogen sites for the detection are still unclear and lack of specialized study. Compared with SWCNTs, double-walled CNTs (DWCNTs) have higher mechanical strength, better chemical stability, and excellent conductivity, hence, doping nitrogen atoms into DWCNTs should be suitable for more sensitive NO₂ detection. Here, we report the comparison of the NO₂ gas-sensing performance based on DWCNTs and N-DWCNTs. The sensor response of the fabricated sensor from N-DWCNTs to NO₂ gas was 2.7-fold higher than that of sensor from DWCNTs. The improvement in the sensor response of N-DWCNTs is attributed to the pyridinic nitrogen site, which has a higher response than the other nitrogen sites.

Dr. W. Muangrat, O. Domanov, Prof. P. Ayala, Prof. T. Pichler, Dr. L. Shi
Electronic Properties of Materials
Faculty of Physics
University of Vienna
Strudlhofgasse 4, 1090 Vienna, Austria
E-mail: lei.shi@univie.ac.at

Dr. W. Wongwiriyan
College of Nanotechnology
King Mongkut's Institute of Technology Ladkrabang
Chalongkrung Road, Ladkrabang, 10520 Bangkok, Thailand

V. Yordsri
National Metal and Materials Technology Center
Phahonyothin Road, Khlong Luang, 12120 Pathumthani, Thailand

T. Chobsilp, S. Inpaeng, Dr. C. Issro
Faculty of Science
Department of Physics
Burapha University
Long-Hard Bangsaen Road, Muang, 20131 Chonburi, Thailand

 The ORCID identification number(s) for the author(s) of this article can be found under <https://doi.org/10.1002/pssa.201800004>.

© 2018 The Authors. Published by WILEY-VCH Verlag GmbH & Co. KGaA, Weinheim. This is an open access article under the terms of the Creative Commons Attribution-NonCommercial License, which permits use, distribution and reproduction in any medium, provided the original work is properly cited and is not used for commercial purposes.

DOI: 10.1002/pssa.201800004

2. Results and Discussion

To reveal the nanostructure of DWCNTs and N-DWCNTs, Transmission electron microscope (TEM) was applied for statistics research. As shown in **Figure 1a** and **b** and S1, Supporting Information, the DWCNTs and the N-DWCNTs are normally in bundles. Sometimes, individual DWCNTs can be seen as shown in the inset of **Figure 1a** and **b**, whose structures are very well and without big defects. Also, no difference of the structure can be found between doped and undoped tubes. The diameter distribution histograms statistically from many TEM images are studied and summarized in **Figure 1c** and S2, Supporting Information. The average diameters of DWCNTs (1.94 ± 0.28 nm) is slightly larger than all the N-DWCNTs synthesized at different temperatures, which implies that the nitrogen doping plays a role in decrease of the diameter of N-DWCNTs. However, in general all the samples have similar diameter distributions. In addition, after purification, the iron catalysts and amorphous carbon were almost completely removed in the DWCNT sample (**Figure 1a**), while in the N-DWCNTs the metal catalytic particles (small particles with darker contrast) and amorphous carbon attached on the wall of tubes can still be found (**Figure 1b** and S1, Supporting Information). Since the amount of amorphous carbon is rather small, and its resistance is much higher than the carbon nanotubes, hence in general the amorphous carbon has almost no influence on the sensor response of the whole sample. Previous work showed that the iron catalyst was insensitive to NO_2 gas.^[19] Therefore, in our case such amount of catalysts will not be considered later in the analysis.

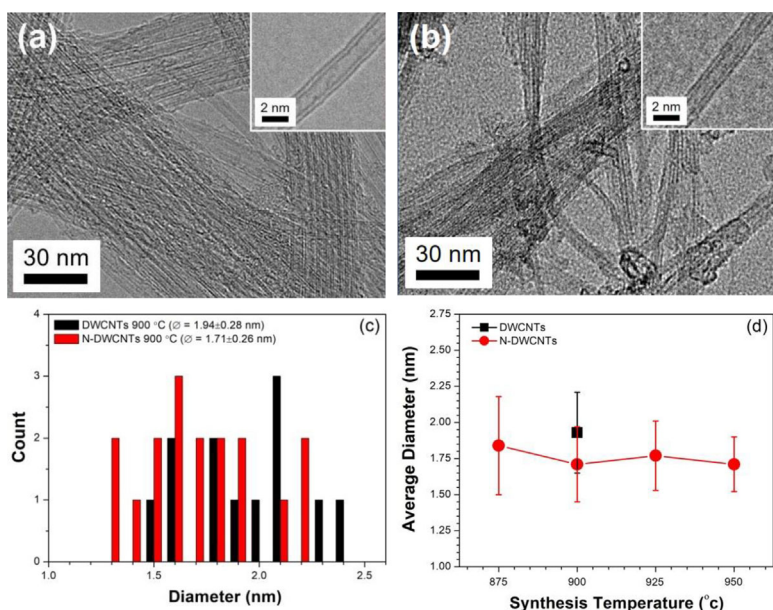


Figure 1. The low- and high-magnification (inset) TEM images of (a) DWCNTs 900 °C and (b) N-DWCNTs 900 °C. (c) Diameter distributions of DWCNTs 900 °C and N-DWCNTs 900 °C obtained from the TEM statistics. (d) The average outer tube diameter of DWCNTs and N-DWCNTs as a function of synthesis temperature obtained from TEM statistics.

Since TEM is a very local measurement, and the purity as well as defects can not be clearly resolved in the TEM, Raman spectroscopy with larger examine area was employed for the DWCNTs and N-DWCNTs samples. First, as seen in **Figure 2a**, no shift of the RBM frequency can be observed, suggesting that the diameter of the tubes are not changed by the N-doping and under different synthesis temperature, which is consistent with the above-mentioned TEM results. Second, compared to the 2D-band of the undoped DWCNTs (**Figure 2b**), the 2D-bands of the N-DWCNTs shift to lower frequencies, which confirms the success of N-type doping.^[20,21] Third, usually, the intensity ratio of the G-band to D-band (I_G/I_D) can be used as indicator of the defects and the impurities. As seen in **Figure 2a**, compared to the DWCNTs ($I_G/I_D = 61.32$), a significant I_G/I_D decrease (**Table S1**, Supporting Information) for all the N-DWCNTs indicates the effects of the N-doping (like defects) and the existence of the impurities. Furthermore, for the N-DWCNTs the change of the I_G/I_D value should be related to the N doping ratio in the samples,^[22] so the samples were measured by X-ray photoelectron spectroscopy (XPS) to obtain the corresponding information about the types of N-doping and their ratios.

C1s peak and O1s peak (introduced during the purification process) can be clearly seen in the survey for both DWCNTs–925 °C and N-DWCNTs–925 °C, and a small peak belong to the N1s can be found in the N-DWCNTs sample (**Figure 3a**). Although the iron catalysts were observed in the TEM, no iron signal can be found in the XPS during the same measurement time as N1s. The C1s is not shifted and also not broadened by the doping, suggesting a low-doping ratio. Indeed, the N-doping ratio is between 0.7 and 1.6 at.% in the samples synthesized at different temperatures (see details in **Table S2**, Supporting Information). Furthermore, four types of nitrogen can be assigned in the samples: pyridinic at 398.2 eV, pyrrolic at 399.9 eV, graphitic at 401.6 eV, and oxidized at 403.7 eV (**Figure 3b**).^[23,24] **Figure 3c** shows the nitrogen content as a function of synthesized N-DWCNTs under 875–950 °C, where 900 °C is the optimized condition to obtain the highest nitrogen concentration of N-DWCNTs. This is consistent with the Raman spectral results that the N-DWCNTs–900 °C sample has lowest I_G/I_D . Hence we confirmed that higher nitrogen content in N-DWCNTs decreases the degree of crystallinity in their structure, resulting in a decrease of I_G/I_D value. Therefore, by different synthesis temperature, we can control the crystallinity and the nitrogen content, which are the key factors for the following sensor sensitivity performance.

The sensors were fabricated from the samples with 0.0–1.6 at.% doping ratio and tested using the sensor response (%) as a function of time at 500 ppm of NO_2 (**Figure 4a**). The electrical resistance of all sensors decreased upon NO_2 exposure. The sensor response of N-DWCNTs–900 °C shows the highest response to NO_2 , which is 2.7-fold higher than that of DWCNTs–900 °C. This result is obvious because

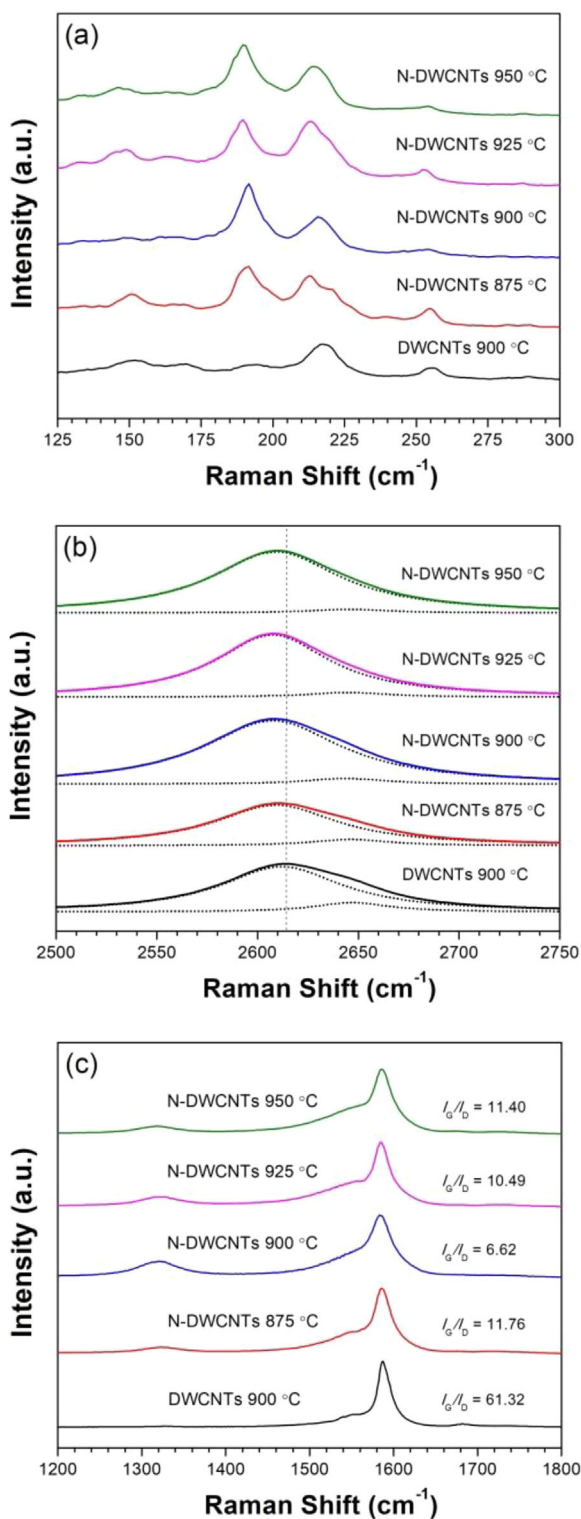


Figure 2. Raman spectra of DWCNTs and N-DWCNTs excited by 633 nm laser. a) RBM region, (b) 2D-band, and (c) G-band and D-band.

the N-DWCNTs–900 °C has the highest doping ratio among the samples. Generally, the sensing mechanism is ascribed to the charge transfer between the absorbed gas molecules and the sensing material. The electron transfers from the DWCNTs/the

N-DWCNTs to NO₂ molecules, then the hole density in the DWCNTs and N-DWCNTs increase (the Fermi level shifts closer to the valence band), resulting in a decrease of the electrical resistance.^[16,18,25] However, the question is which type of N-doping plays greater role in the sensing process? To answer this, Figure 4b shows the sensor response of all sensors toward 500 ppm of NO₂ as a function of nitrogen type. It shows that the sensor response of N-DWCNTs depends strongly on the amount of pyridinic nitrogen in N-DWCNTs but not the amount of pyrrolic nitrogen, because the adsorbed NO₂ molecules more favor at the pyridinic site compared to the other nitrogen sites, resulting in the highest response for N-DWCNTs–900 °C.^[26] In addition, several stages exist in the response curve, because the response speed varies for defects and functional groups on the nanotubes as well as different types of nitrogen sites.

For the recovery of sensor, all sensors were unable to recovery to their initial resistance by N₂ gas purging (data not shown). NO₂ molecule strongly interact with sensing materials through chemisorption, resulting in difficulty in removing NO₂ molecules from the sensing materials.^[27,28] The reversibility of the sensor can be improved by applying heat or UV exposure, similar to the SWCNT sensor system.^[8–10] For the response time of the sensor, the response time is defined as the time taken by the sensor to reach 90% of its maximum sensor response. The DWCNTs 900 °C showed the fastest response with a response time of ≈278 s, but it exhibited the smallest response magnitude. On the other hand, the N-DWCNTs 900 °C enabled threefold improvement in NO₂ detection compared to the DWCNTs 900 °C. However, the response time of the N-DWCNTs 900 °C increased up to 791 s, which is ≈2.85 times higher than that of the pristine DWCNTs. The N-DWCNTs 900 °C shows a merit for a significant enhancement of sensor response magnitude but there is room for improvement in its response time.

Another key factor for the sensor is the limit of detection (LOD). **Figure 5** shows the sensor response of N-DWCNT–900 °C as function of time and NO₂ concentration in the range of 5–500 ppm. The sensor response N-DWCNT–900 °C increases with the NO₂ concentration (Figure 5a), and trends to saturate at 500 ppm (Figure 5b), because the sensing material surface is completely covered by NO₂ molecule to avoid any more exposure. The feature of NO₂ adsorption can be described based on the Langmuir isotherm.^[9,29] The calculation of LOD of N-DWCNTs–900 °C is investigated, and 10 consecutive data points prior to exposure to NO₂ were plotted to fit a fifth-order polynomial. The V_{x^2} was calculated using Equation (1), where y_i is the measured value of sensor response and y is the corresponding value calculated from the fifth-order polynomial fit. Equation (2) was used to calculate the rms_{noise} of the sensor, where N is the number of data points used for the curve fitting ($N = 30$). Finally, the LOD can be obtained from Equation (3) by the slope of the linear regression fit on the sensor response versus concentration plot.^[8] The calculated LOD of N-DWCNTs–900 °C is 0.14 ppm. Compared to the sensor performance based on SWCNTs and MWCNTs at room temperature, our result shows lower LOD by the help of pyridinic N-doping.^[6,30]

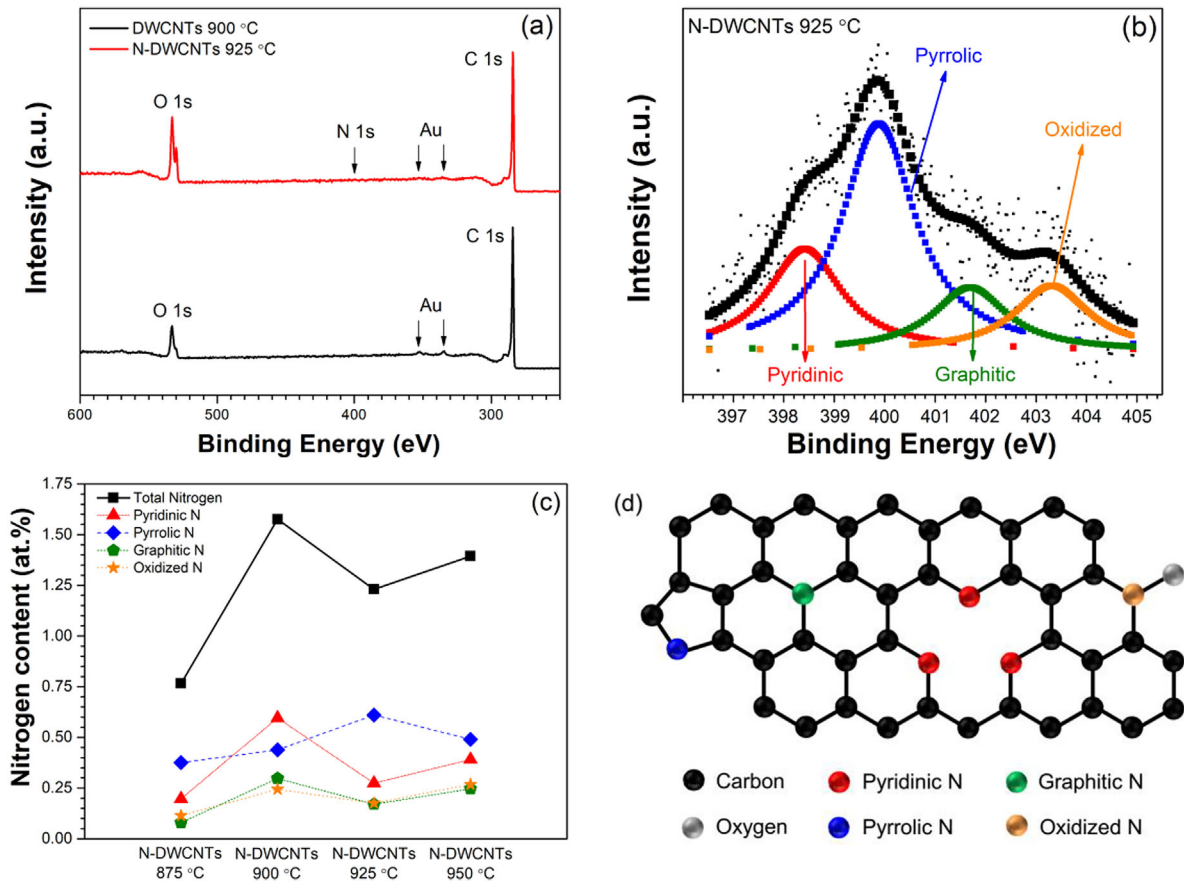


Figure 3. a) XPS survey of DWCNTs 900 °C and N-DWCNTs 925 °C. b) The N 1s spectra of N-DWCNTs 925 °C. c) The nitrogen content as a function of synthesized N-DWCNTs at 875–950 °C. d) Schematic view of different types of nitrogen doping sites.

These results imply that the sensor based on N-DWCNTs–900 °C could be down to part per billion-level NO₂ detection in future if combined with functionalization by Pt, Pb, Au, and with other substrate.^[31–33]

$$\text{rms}_{\text{noise}} = \sqrt{\frac{V_{x^2}}{N}} \quad (2)$$

$$V_{x^2} = \sum (y_i - y)^2 \quad (1) \quad \text{LOD} = 3 \frac{(\text{rms}_{\text{noise}})}{\text{slope}} \quad (3)$$

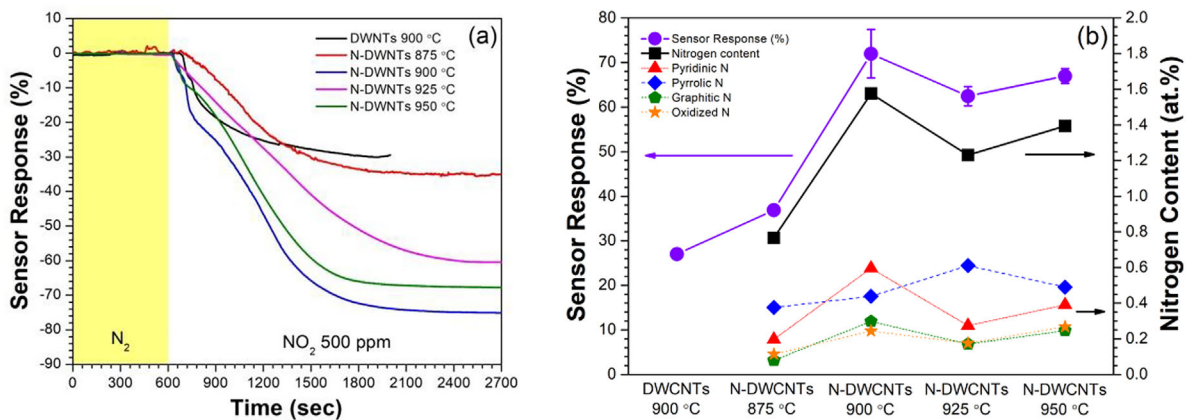


Figure 4. a) Sensor responses (%) of all sensors toward 500 ppm of NO₂ as a function of time. b) Sensor response saturation limit (left axes) and the ratio of different types of nitrogen as a function of synthesized temperature.

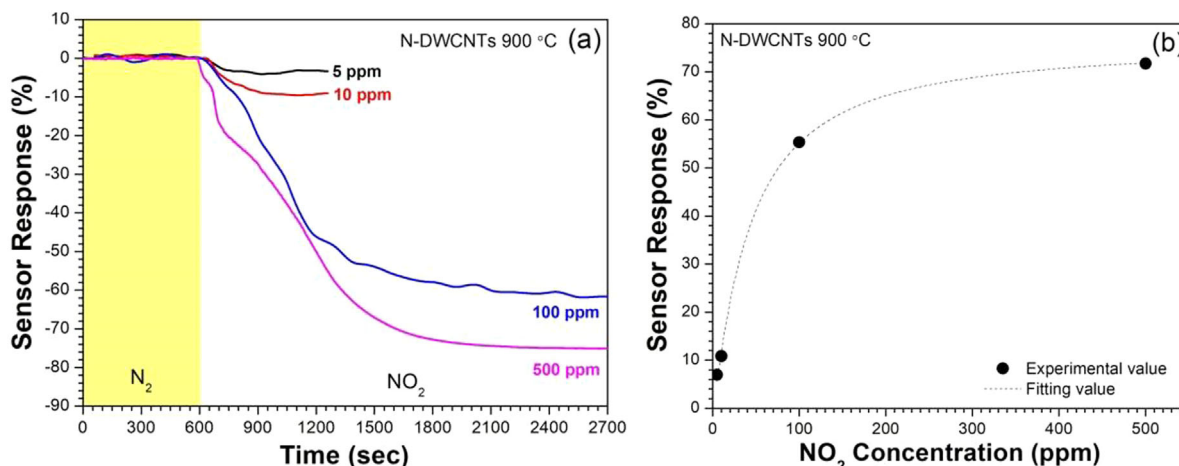


Figure 5. Sensor responses (%) of N-DWCNTs 900 °C as a function of (a) time, and (b) NO₂ concentration in the range of 5–500 ppm.

3. Conclusions

The NO₂ gas sensors were fabricated based on N-DWCNTs with different types of nitrogen doping and various doping ratio, and their performances were tested and compared to the sensor made from DWCNTs. The results show that the N-DWCNTs–900 °C exhibited a 2.7-fold improvement in the response to NO₂ gas compared to DWCNTs–900 °C, which is attributed to the charge transfer from sensing materials to the adsorbed NO₂ molecule. Importantly, the pyridinic nitrogen was proved that it plays greater role than the other types of nitrogen of N-DWCNTs in improving the sensor performance. Furthermore, following the Langmuir adsorption isotherm, the LOD of the optimum sensor is 0.14 ppm NO₂, which is much improved compared to the undoped DWCNTs. Therefore, it is very promising to be used in real NO₂ detection at room temperature in future.

4. Experimental Section

Synthesis of DWCNTs and N-DWCNTs: DWCNTs and N-DWCNTs were synthesized by HVCVD using reported method.^[34–36] The DWCNTs and N-DWCNTs were grown using ethanol (Sigma–Aldrich) as the carbon source and benzylamine (Sigma–Aldrich) as the carbon and nitrogen sources, respectively. Firstly, ammonium iron (III) citrate (Fluka) at the concentration of 3 wt.% was mixed with magnesium oxide (MgO, Sigma–Aldrich) nanostructured powders in ethanol by sonication for 30 min and followed by stirred by Heating ThermoMixer (DITABIS, MHR 13, V 301A4) at the rotation speed of 3000 rounds per minute at 70 °C for 24 h in order to remove the ethanol. The mixed powder was ground to obtain a fine catalyst powder and placed in an alumina crucible which placed horizontally in the center of the HVCVD. The base pressure was evacuated to 10^{–7} mbar and then the temperature was increased to 400 °C to eliminate the humidity in the catalysts until the pressure reached back to 10^{–7} mbar. The synthesis temperature was carried out in the range of 875–950 °C (referred to as DWCNTs–900 °C, N-DWCNTs–875 °C, N-DWCNTs–900 °C, N-DWCNTs–925 °C, and N-DWCNTs–950 °C, respectively). To synthesize DWCNTs/N-DWCNTs, ethanol/benzylamine vapors were introduced into HVCVD system controlled by a needle valve to keep the pressure at ≈50–70 and ≈1 mbar, respectively, keeping

the synthesis for 60 min. Then, the HVCVD was cooled down to room temperature with high vacuum to avoid the amorphous carbon formed. The as-grown samples were immersed in 37% hydrochloric (HCl) acid for 12 h, then filtered and washed with distilled water until pH = 7. Next, the samples were annealed under air atmosphere at 400 °C for 30 min to remove the covered amorphous carbon attached on the tubes and the catalysts. Then again samples were soaked in 37% of HCl acid for 12 h, filtered, and washed with distilled water until pH = 7. Finally, the samples were annealed under air atmosphere at 500 °C for 30 min to remove the SWCNTs.

Characterization Techniques: Raman spectroscopy (Horiba JobinYvon, LabRAM HR800) was employed to characterize the purity and crystallinity with 633 nm (1.96 eV) wavelength light from an Ar laser light source. The nanostructure was analyzed by transmission electron microscopy operated at 200 KV (TEM; JEOL, JEM-2100). The chemical bonding and element composition were characterized by X-ray photoelectron spectroscopy (XPS) using hemispherical SCIENTA RS4000 photoelectron equipped with a monochromatic Al K_α radiation (1486.7 eV).

Fabrication of Sensor Devices and Gas Sensor Measurement: A total of 1 mg of purified DWCNTs and N-DWCNTs suspension were separately dispersed in 25 mL of ethanol by ultra-sonication for a designated time period. A 100 μL of DWCNTs–900 °C, N-DWCNTs–875 °C, N-DWCNTs–900 °C, N-DWCNTs–925 °C, and N-DWCNTs 950 °C in ethanol were separately dropped onto the ceramic substrate. During drop casting the substrate was heated at 100 °C to eliminate the solvent in the sample material. The sensor response to NO₂ gas was investigated at room temperature by recording their electrical resistance using multimeter (FLUKE 189). The changing of electrical resistance measurement was performed using a four-point probe method. The fabricated all sensors were placed in the stainless steel chamber and then N₂ gas was introduced into the chamber at a flow rate of 500 standard cubic centimeters per minute (sccm) for 10 min as a baseline. The mixed NO₂ and N₂ gas was introduced into the detection chamber to measure the sensor response of all sensors. The NO₂ concentration was in the range of 5–500 ppm which adjusted by the flow rate of NO₂ and N₂ dilution gas. All of sensors were measured until to reach its saturation point. The sensor response (SR) (%) of all sensors was calculated following by Equation (4), where R_{NO₂} and R_{N₂} are the electrical resistances of the sensor after and before NO₂ exposure, respectively.

$$SR(\%) = \left(\frac{R_{NO_2} - R_{N_2}}{R_{N_2}} \right) \times 100 \quad (4)$$

Supporting Information

Supporting Information is available from the Wiley Online Library or from the author.

Acknowledgments

This work was financially supported by the Austrian Federal Ministry for Science and Research in the frame of the ASEA UNINET, and National Research Council of Thailand (NRCT). Lei Shi and Thomas Pichler thank the EU project (2D-INK 664878).

This article was amended on August 13, 2018 to correct the copyright byline.

Conflict of Interest

The authors declare no conflict of interest.

Keywords

gas sensors, nitrogen-doped double-walled carbon nanotubes, nitrogen dioxide, pyridinic nitrogen

Received: January 2, 2018

Revised: March 6, 2018

Published online: April 25, 2018

-
- [1] S. Iijima, *Nature* **1991**, 354, 56.
 [2] S. Iijima, T. Ichihashi, *Nature* **1993**, 363, 603.
 [3] M. S. Dresselhaus, G. Dresselhaus, J. C. Charlier, E. Hernandez, *Philos. Trans. R Soc. Lond. A* **2004**, 362, 2065.
 [4] A. Peigney, C. Laurent, E. Flahaut, R. R. Bacsa, A. Rousset, *Carbon* **2001**, 39, 507.
 [5] C. Subramaniam, T. Yamada, K. Kobashi, A. Sekiguchi, D. N. Futaba, M. Yumura, K. Hata, *Nat. Commun.* **2013**, 4, 2202.
 [6] J. Kong, N. R. Franklin, C. Zhou, M. G. Chapline, S. Peng, K. Cho, H. Dai, *Science* **2000**, 287, 622.
 [7] C. Cantalini, L. Valentini, I. Armentano, L. Lozzi, J. M. Kenny, S. Santucci, *Sens. Actuat. B* **2003**, 95, 195.
 [8] J. Li, Y. Lu, Q. Ye, M. Cinke, J. Han, M. Meyyappan, *Nano Lett.* **2003**, 3, 929.
 [9] W. Wongwiriyan, S. Honda, H. Konishi, T. Mizuta, T. Ikuno, T. Ito, T. Maekawa, K. Suzuki, H. Ishikawa, K. Oura, M. Katayama, *Jpn. J. Appl. Phys.* **2005**, 44, L482.
 [10] I. Sayago, H. Santos, M. C. Horrillo, M. Aleixandre, M. J. Fernandez, E. Terrado, I. Tacchini, R. Aroz, W. K. Maser, A. M. Benito, M. T. Martinez, J. Gutierrez, E. Munoz, *Talanta* **2008**, 77, 758.
 [11] P. Qi, O. Vermesh, M. Grecu, A. Javey, Q. Wang, H. Dai, S. Peng, K. J. Cho, *Nano Lett.* **2003**, 3, 347.
 [12] T. Zhang, S. Mubeen, E. Bekyarova, B. Y. Yoo, R. C. Haddon, N. V. Myung, M. A. Deshusses, *Nanotechnology* **2007**, 18, 165504.
 [13] A. Star, V. Joshi, S. Skarupo, D. Thomas, J. C. P. Gabriel, *J. Phys. Chem. B* **2006**, 110, 21014.
 [14] Y. Lu, C. Partridge, M. Meyyappan, J. Li, *Electroanal. Chem.* **2006**, 593, 105.
 [15] M. Penza, G. Cassano, R. Rossi, M. Alvisi, A. Rizzo, M. A. Signore, T. Dikonimos, E. Serra, R. Giorgi, *Appl. Phys. Lett.* **2007**, 85, 666.
 [16] F. Villalpando-Páez, A. H. Romero, E. Munoz-Sandoval, L. M. Martinez, H. Terromes, M. Terromes, *Chem. Phys. Lett.* **2004**, 386, 137.
 [17] J. J. Adjizian, R. Leghrib, A. A. Koos, I. Suarez-Martinez, A. Crossley, P. Wagner, N. Grobert, E. Llobet, C. P. Ewels, *Carbon* **2014**, 66, 662.
 [18] Y. Battie, O. Ducloux, P. Thobois, T. Susi, E. I. Kauppinen, A. Loiseau, *Phys. Status Solidi B* **2011**, 248, 2462.
 [19] L. C. Wang, K. T. Tang, I. J. Teng, C. T. Kuo, C. L. Ho, H. W. Kuo, T. H. Su, S. R. Yang, G. N. Shi, C. P. Chang, *Sensors* **2011**, 11, 7763.
 [20] R. Pfeiffer, H. Kuzmany, F. Simon, S. Bokova, E. Obratsova, *Phys. Rev. B* **2005**, 71, 155409.
 [21] J. F. Cardenas, *Chem. Phys. Lett.* **2006**, 430, 367.
 [22] C. Xiong, Z. Wei, B. Hu, S. Chen, L. Li, L. Guo, W. Ding, X. Liu, W. Li, X. Wang, *J. Power Sources* **2012**, 215, 216.
 [23] T. Susi, T. Pichler, P. Ayala, *Beilstein J. Nanotechnol.* **2015**, 6, 177.
 [24] L. G. Bulusheva, E. O. Fedorovskaya, A. G. Kurenaya, A. V. Okotrub, *Phys. Status Solidi B* **2013**, 250, 2586.
 [25] L. Bai, Z. Zhou, *Carbon* **2007**, 45, 2105.
 [26] Y. S. Min, E. J. Bae, U. J. Kim, E. H. Lee, N. Park, C. S. Hwang, W. Park, *Appl. Phys. Lett.* **2008**, 93, 043113.
 [27] W. L. Yim, X. G. Gong, Z. F. Liu, *J. Phys. Chem.* **2003**, 107, 9363.
 [28] L. Valentini, F. Mercuri, I. Armentano, C. Cantalini, S. Picozzi, L. Lozzi, S. Santucci, A. Sgamellotti, J. M. Kenny, *Chem. Phys. Lett.* **2004**, 387, 356.
 [29] K. Oura, V. G. Lifshits, A. A. Saranin, A. V. Zotov, M. Katayama, *Surface Science—An Introduction*. Springer, Berlin **2003**.
 [30] P. G. Su, C. T. Lee, C. Y. Chou, K. H. Cheng, Y. S. Chuang, *Sens. Actuat. B: Chem.* **2009**, 139, 488.
 [31] M. Penza, G. Cassano, R. Rossi, M. Alvisi, A. Rizzo, M. A. Signore, E. Serra, R. Giorgi, *Sens. Actuat. B: Chem.* **2008**, 135, 289.
 [32] Z. Zanolli, R. Leghrib, A. Felten, J. J. Pireaux, E. Llobet, J. C. Charlier, *ACS Nano* **2011**, 5, 4592.
 [33] S. W. Choi, J. Kim, Y. T. Byun, *Sens. Actuat. B: Chem.* **2017**, 238, 1032.
 [34] P. Ayala, A. Grüneis, T. Gemming, D. Grimm, C. Kramberger, M. H. Rummeli, F. L. Freire, H. Kuzmany, R. Pfeiffer, A. Barreiro, B. Büchner, T. Pichler, *J. Phys. Chem. C* **2007**, 111, 2879.
 [35] L. Shi, M. Sauer, O. Domanov, P. Rohringer, P. Ayala, T. Pichler, *Phys. Status Solidi B* **2015**, 252, 2558.
 [36] L. Shi, P. Rohringer, K. Suenaga, Y. Niimi, J. Kotakoski, J. C. Meyer, H. Peterlik, M. Wanko, S. Cahangirov, A. Rubio, Z. J. Lapin, L. Novotny, P. Ayala, T. Pichler, *Nat. Mater.* **2016**, 15, 634.